Tuning sound transmission loss for multi-layer panels with aniso-tropic foams

E. Lundberg [1,2,4], **H. Mao** [1,2], **M. Gaborit** [1,2,3], **R. Rumpler** [1,2], **B.P. Semeniuk** [1], **P. Göransson** [1,2]
[1] KTH Royal Institute of Technology, Department of Engineering Mechanics, MWL
Stockholm, Sweden
e-mail: **eval@kth.se**

[2] KTH Royal Institute of Technology, The Centre for ECO2 Vehicle Design
Stockholm, Sweden

[3] Le Mans Universit´e, CNRS, LAUM, UMR 6613, IA-GS,
Le Mans, France

[4] Volvo Construction Equipment,
Eskilstuna,Sweden

Abstract
Multilayer panels consisting of a load carrying structure, a porous material for thermal and acoustic insulation and an interior trim panel is a very common type of design for vehicles. Weight as well as total build height are usually limiting constraints on the design. The idea of using an anisotropic porous material instead of an isotropic one to improve the sound transmission loss without adding a lot of weight or thickness is explored in the paper. By using a state space formulation of the transfer matrix method transmission loss it is possible to include anisotropic material properties in the calculation. The anisotropic material is modelled by a combination of a simplified analytical model for the acoustic losses and inverse estimation of the 21 independent elastic constants of the Hooke's tensor. The porous material, which has typical dimensions possible to 3D print, is based on a Kelvin cell micro model that has a controlled degree of anisotropy.

1 Introduction

Estimating Sound Transmission Loss (STL) of multi-layer panels using Transfer Matrix Method (TMM) is a standard method for noise and vibration control. The most widely used method, which also is referenced as the Thompson Haskell method has the disadvantage of becoming unstable for certain types of problems and frequency ranges [1]. A more stable transfer matrix method based on a state space formulation was proposed by Dazel et al. [1] and was implemented by Parra Martinez [2] for multi-layer panels including porous materials. It was demonstrated that this method, unlike the classical Thomson-Haskell method [3, 4], also can include layers with anisotropic properties. In Parra Martinez analysis [2], a multilayer panel consisting of an anisotopic porous material between two thin flat metal plates was carried out. The anisotropic data of the foam in Ref. [5] was obtained using experimental characterizations in combination of inverse methods for both acoustic and stiffness properties of a slightly anisotropic melamine foam. It is possible to find several good examples of characterizations of transverse isotropic porous materials like fiber materials. Huber and Gibson pointed out the importance of including anisotropic properties with regard to mechanical properties of cellular materials [6]. Among recent work based on micro geometry approaches of anisotropic porous materials can Jonkers et al. [7] who studied anisotropic food stuffs, and Cavalieri et al.[8] focussing on absorption of anisotropic and graded porous materials be mentioned. One example of an anisotropic porous material that is not transverse isotropic is the analysis by Luu et al. [9] of a fibre material including the out of plane distribution of fibers. For the stiffness properties finite element calculations in combination with inverse

characterizations have proven to work well as demonstrated by Mao et al. [10, 11], e.g., for anisotropic foams including effects such as auxetic behaviour and compression-shear coupling. For the acoustic properties of the porous material the numerical analysis with thermo-viscous fluid is computationally very demanding, but experimental setups for a complete anisotropic acoustic experimental characterization are few [5, 9] . Due to the development of 3D printing technology, the analysis of anisotropic materials is no longer restricted to the traditional fiber materials or chemically foamed materials. The new techniques offer possibilities of designing a material with defined properties, and thereby a practical option to investigate anisotropic porous materials. This need is the motivation for the present work, where a fast analytical method only requiring a few micro parameters to estimate the acoustic properties is developed and used together with the inverse characterisation method for anisotropic material stiffness properties. The intended use of the method is to use it in an early phase in order to assess a number of possible designs in order to select the most promising candidates for later manufacturing and detailed characterization. Examples of approaches for detailed characterization of isotropic materials can for instance be found in [12]. The goal with the proposed method is to select the designs best tuned to the specific conditions with regard to excitation frequencies and physical limitations such as total weight or build height, including options of using anisotropic porous materials in the multilayer design.

The paper is organised as follows. In Section 2, the governing equations for the porous material are stated. The methods for estimating both acoustic and mechanical stiffness properties are presented in Section 3, and validated in Section 4. Then, applications in tuning the sound transmission loss of panels with anisotropic foam are introduced in Section 5 and some interesting results are presented in Section 6. Some remarks for future considerations are discussed in Section 7. Finally, some conclusions are provided in Section 8.

2 Governing equations for the micro modelled foam

The governing equations for the porous material are first stated in a classical Biot formulation, expressed in $\{\boldsymbol{u^s}, \boldsymbol{u^t}\}$ formulation in terms of solid displacements $\boldsymbol{u^s}$ and total displacements $\boldsymbol{u^t}$, developed according to Dazel et al. [13]. The governing equations will then be

$$\nabla \hat{\boldsymbol{\sigma}}^s = -\omega^2 \tilde{\boldsymbol{\rho}}_s \boldsymbol{u^s} - \omega^2 \tilde{\boldsymbol{\tau}} \boldsymbol{u^t} \tag{1}$$

$$-\nabla p = -\omega^2 \tilde{\boldsymbol{\tau}} \boldsymbol{u^s} - \omega^2 \tilde{\boldsymbol{\rho}}_{eq} \boldsymbol{u^t} \tag{2}$$

$$\boldsymbol{u}^t = (1-\phi)\boldsymbol{u}^s + \phi \boldsymbol{u}^f \tag{3}$$

$\boldsymbol{\tau}$ is the tensor corresponding to the scalar expression of $\tilde{\gamma}\tilde{\rho}_{eq}$ used for isotropic materials. The fluid and solid part are described by the constitutive equations

$$p = -\tilde{K}_{eq} \nabla \boldsymbol{u^t} \tag{4}$$

$$\hat{\boldsymbol{\sigma}}^s = \boldsymbol{C}\boldsymbol{\epsilon^s}, \tag{5}$$

where $\hat{\boldsymbol{\sigma}}^s$ is the in vacuo stress tensor for the material, $\boldsymbol{C}$ is the Hooke's tensor and $\boldsymbol{\epsilon^s}$ is the strain tensor. $\tilde{K}_{eq}$ in equation 4 is dynamic equivalent bulk modulus.

If the governing equations are instead expressed including the dynamic drag impedance $\boldsymbol{Z}$ following Semeniuk's derivation for fibre materials [14], for a foam material where strut length is explicitly included, these expressions will be

$$\nabla(\boldsymbol{\sigma^s}) = (1-\phi)\boldsymbol{\rho_s}\ddot{\boldsymbol{u}}^s + \boldsymbol{Z}(\dot{\boldsymbol{u}}^{\boldsymbol{s}} - \dot{\boldsymbol{u}}^{\boldsymbol{f}}) \tag{6}$$

$$-\phi \nabla p \boldsymbol{I} = \phi \boldsymbol{\rho_f} \ddot{\boldsymbol{u}}^f + + \boldsymbol{Z}(\dot{\boldsymbol{u}}^{\boldsymbol{f}} - \dot{\boldsymbol{u}}^{\boldsymbol{s}}) \tag{7}$$

The dynamic drag impedance $\boldsymbol{Z}$ is a quantity relating the of the dynamic frequency dependent viscous drag force to the relative velocity between fluid and solid [14, 15],

$$\boldsymbol{F_D} = \boldsymbol{Z}(\dot{u}^s - \dot{u}^f). \tag{8}$$

where $\boldsymbol{F_D}$ is the force the solid skeleton exerts on the fluid. Due to symmetry it also relates the viscous forces exerted by the fluid on the solid.

Re-writing equations 7 and 6 with collecting the terms proportional to $\boldsymbol{u^s}$ and $\boldsymbol{u^t}$, the expressions corresponding to $\tilde{\boldsymbol{\rho}}_{eq}$, $\tilde{\boldsymbol{\rho}}_{eq}\tilde{\gamma}$ and $\tilde{\boldsymbol{\rho}}_{\boldsymbol{s}}$ can be identified as

$$\tilde{\boldsymbol{\rho}}_s = (1-\phi)\rho_s \boldsymbol{I} + \frac{(1-\phi)^2}{\phi}\rho_f \boldsymbol{I} - \frac{i\boldsymbol{Z}}{\omega\phi^2} \tag{9}$$

$$\tilde{\boldsymbol{\tau}} = -\frac{(1-\phi)}{\phi}\rho_f \boldsymbol{I} + \frac{i\boldsymbol{Z}}{\omega\phi^2} \tag{10}$$

$$\tilde{\boldsymbol{\rho}}_{eq} = \frac{\rho_f \boldsymbol{I}}{\phi} - \frac{i\boldsymbol{Z}}{\phi^2\omega}. \tag{11}$$

As can be seen from equations 9, 10 and 11, the necessary input based on the micro formulation is limited to porosity, fluid and solid density, and dynamic drag impedance. These in turn depend only on the parameters for the simplified micro geometry, cell height, strut thickness and twist angle in addition to material properties, see Section 3. The constitutive equation for the fluid in the micro model is replaced by the expression for a rigid frame material $p = -K_{eq}\nabla \boldsymbol{u^t}$ with $K_{eq} = K_f/\phi$ that only depends on micro geometry and the properties of air for a rigid frame porous material. This allows for designs including anisotropic micro geometries to be investigated with limited computational resources. The underlying assumption in this model is that the foam is periodic and the bulk material is fully described by the equivalent properties of the unit cell.

3 Micro model for an anisotropic foam

Rather than characterizing the material as a Biot material using common models e.g. the Johnson-Champoux-Allard model (JCA) where parameters must be characterized either from measurements of a physical sample or from computationally demanding numerical models, the acoustics properties are estimated from a simplified micro geometry based on a Kelvin cell (KC). The analytical estimation of the acoustic properties is based on a few micro geometry parameters: cell height, strut thickness and twist angle together with material properties. The twist angle controls the degree of anisotropy. The output from the analytical method is the porosity and the dynamic drag impedance. The dynamic drag impedance $\boldsymbol{Z}$ for the micro structure is a dynamic and frequency dependent estimate related to, but not equal to, the static flow resistivity for a sample. There is not a one to one correspondence between the two models of estimating the viscous losses. The static flow resistivity is quasi-static constant while the dynamic drag impedance is frequency dependent. For an anisotropic material $\boldsymbol{Z}$ will be a 3×3 tensor that may include off-diagonal terms.

3.1 Micro geometry and controlled anisotropy

An isometric KC arrangement exhibiting cubic material symmetry is chosen as the reference micro-structure, named as REF, see Figure 1a. The cell has 6 square and 8 hexagonal faces, arranged in a body-centered cubic lattice. A cellular array built from the KC in this original, isometric, form, has an equivalent linear elastic isotropic Hooke's tensor, characterised by a Young's modulus and a Poisson's ratio [10, 11, 16, 17, 18].

The geometrical modifications applied to the reference geometry are in the form of rigid body rotations of the square faces of REF, and keeping these square undeformed during the rotation, Figure 1. Topologically, the cell is not modified and all vertices remain connected through the same struts (with altered lengths) as in the reference geometry. Thus, the modified cells still form a 3D cellular array as seen in Figure 1c. There are many different ways to apply such rotations as detailed in [11], however in the present contribution only in-plane twisting rotations of the square faces of the KC are considered, as given in Figures 1b–1c. To facilitate

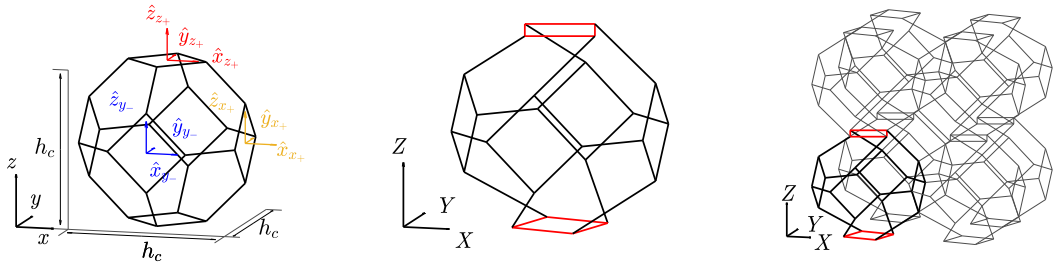

(a) (b) (c)

Figure 1: (a) Reference isometric single KC (REF), in unit cell Cartesian coordinate system xyz, and local square faces coordinate systems $\hat{x}\hat{y}\hat{z}$ with subscripts identifying to which of the square faces it refers; (b) A single auxetic cell generated by twisting local square faces (red color) of the reference KC anti-symmetrically alone Z-axis, named as cell NTw1Az; and (c) 2×2 modified KC array, in global Cartesian coordinate system XYZ.

the discussion, each square face is indicated by its outgoing normal and orientation (positive or negative), see Figure 1, and denoted as $x_-, x_+, y_-, y_+, z_-, z_+$.

The twisting of the KC square faces will potentially break the cubic symmetry of REF. If the twist a pair of faces with a same angle in the same direction e.g. twisting upper and lower square surfaces normal to the Z-axis, the geometry is called symmetrical, and if one of the surfaces are opposite sign to the other the geometry is referred to as anti-symmetric, as shown in Figure 1b. From stiffness point of view the anti-symmetric geometry will have a Hooke's tensor that is close to a transverse isotropic behaviour, while the symmetric geometry will be anisotropic. The focus in this work is on the anti-symmetric geometry twisted only around the vertical Z-axis denoted NTw1Az as shown in Figure 1b.

The anti-symmetric twisted KC exhibits chiral symmetry to each middle-plane that parallel to each pair of twisted faces, as shown in Figure 1b with the chiral symmetry to Z-plane of the single lattice. When a load is applied to the chiral structure, the non-central force or non-affine deformation induce auxetic behavior, as the predicted anisotropic equivalent Hooke's matrix in [11], where the elastic constant of the Hooke's tensor are controlled by the twisting angles and faces.

3.2 Porosity

As the properties per unit volume of the micro model are required for sound transmission loss calculation and the twisting breaks the symmetry of the single cell, the $2 \times 2 \times 2$ super-cell, Figure 1c, is selected instead of the single cell to calculate the micro geometry properties. The total strut volume filling the cube with dimensions $2L_x \times 2L_y \times 2L_z$ corresponds to a total strut volume of 16 unit cells. Therefore the porosity is estimated as $\phi = 1 - (16V_{s,cell})/(8L_xL_yL_z)$. $V_{s,cell}$ denotes the volume of struts in one unit cell with 24 struts including the joints.

Since the porosity will be included in all calculated properties given per unit volume the accuracy of the strut volume will directly affect the accuracy of all other estimated properties. For foams with a high porosity of more than 99% the overlap at joints and between struts can be neglected without causing substantial errors. However, for structures with lower porosity such as the foams considered here with typical dimensions of 3D printed foams it is essential to estimate the total strut volume as accurately as possible.

Figure 2 shows, from each strut i with angles θ_{i1} and θ_{i2} to the adjoining struts, the volume of the spherical joints is removed as well as the overlap between the adjoining struts. The total strut volume in one unit cell including the volume of the 12 full spherical joints is

$$V_{s,cell} = 12\frac{4\pi r_i^3}{3} + \sum_{i=1}^{24} \pi r_i^2 l_i - \left(\frac{\pi r_i^3}{4\tan(\theta_{i1}/2)} + \frac{\pi r_i^3}{4\tan(\theta_{i2}/2)}\right) - \frac{4\pi r_i^3}{3}\left(\frac{1}{2} + \frac{\theta_{i1}/2}{2\pi} + \frac{\theta_{i2}/2}{2\pi}\right) \quad (12)$$

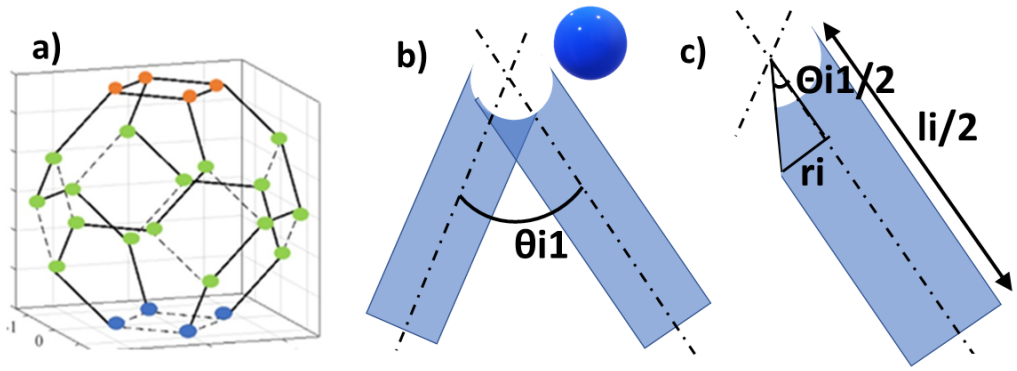

Figure 2: Model for calculating the porosity. a) Unit cell with 24 struts including joints, where only a volume corresponding to 12 full joints belong to the unit cell. b) Overlap between two struts that is removed is marked in darker shade c) Part of a half strut included in porosity calculation.

where the angle θ_1 is the angle to the adjoining strut in one end and θ_2 is the angle to the adjoining strut in another end of strut i.

3.3 Acoustic losses

The method for how to estimate the dynamic drag impedance for an isometric Kelvin cell was presented by Lundberg et al. in [19] and the derivation of the expressions can be found in Semeniuk [14]. In this paper, the methods are extended to anisotropic cellular structures for estimation of the dynamic drag impedance. With the objective of finding a fast and simple way of estimating the dynamic drag impedance several assumptions have been made. The struts are assumed to be rigid and to have circular cross section. The air is assumed to be viscous and in-compressible under the condition that the micro unit cell is much smaller than both the sample size and the wavelength of air. The fundamental assumption that makes it possible to calculate an anisotropic micro geometry with less computational effort is that the interaction between the struts is neglected. At the very lowest quasi-static frequencies, interaction of the viscous loss regions on the surface of neighbouring struts could influence the results for dense materials [14, 20, 12, 21]. That may lead to an underestimation of the dynamic drag impedance at lower frequencies. This simplification is considered acceptable as this analytical approach is not primarily developed for detailed investigations, but rather for exploring a design space including many different designs. It does however, unlike the classical JCA model, allow for analyzing anisotropic porous materials, and is in addition to that a fast way to estimate the acoustic losses that is not computationally demanding. Thus the dynamic drag impedance for anisotropic cell derived from Refs. [19, 14] is

$$\boldsymbol{Z_{cell}} = \begin{bmatrix} Z_{11} & Z_{12} & Z_{13} \\ Z_{12} & Z_{22} & Z_{23} \\ Z_{13} & Z_{23} & ZZ_{33} \end{bmatrix} = \frac{1-\phi}{V_s} \sum_{i=1}^{N} \boldsymbol{R_i} \begin{bmatrix} Z_{Li} & 0 & 0 \\ 0 & Z_{Ti} & 0 \\ 0 & 0 & Z_{Ti} \end{bmatrix} \boldsymbol{R_i^T}. \tag{13}$$

where

$$Z_{Li} = 2\pi \int_0^{l_i} r_i k_\beta \mu_f \frac{H_1^{(2)}(k_\beta r_i)}{H_0^{(2)}(k_\beta r_i)} dz = 2\pi r_i l_i k_\beta \mu_f \frac{H_1^{(2)}(k_\beta r_i)}{H_0^{(2)}(k_\beta r_i)} \tag{14}$$

$$Z_{Ti} = i\pi r_i^2 l_i \rho_f \omega \Big(1 - \frac{4H_1^{(2)}(k_\beta r_i)}{k_\beta r_i H_0(2)(k_\beta r_i)}\Big) \tag{15}$$

$\boldsymbol{R_i}$ is the rotation matrix to rotate the strut from the local coordinate system aligned with the strut to the global coordinate system. Z_{Ti} represents the losses from a transverse flow across strut i, and Z_{Ti} the losses

from a flow longitudinally along the length of strut i. $k_\beta = \sqrt{-(i\omega\rho_f/\mu_f}$ is the shear wave number for the viscous fluid.

3.3.1 Dynamic drag impedance for the anisotropic micro modelled foam

The foam in the example is the micro-geometry denoted NTw1Az, Figures 1b–1c, of different anti-symmetric twisting angles, e.g., with $30°$, $46°$, and $60°$. Figures 1b–1c. The resulting dynamic drag impedance estimated at 20 Hz is given in Table 1.

Table 1: Components of the dynamic drag impedance for the NTw1Az case with varying degree of twist. All unit cells have cell height 3mm and strut diameter 0.5mm.

Model	twist angle	Z_{11}	Z_{22}	Z_{33}	Z_{12}	Z_{13}	Z_{23}	porosity
–	°	Ns/m^4	Ns/m^4	Ns/m^4	Ns/m^4	Ns/m^4	Ns/m^4	–
NTw1AZ	0	333	333	333	0	0	0	0.7025
NTw1AZ	30	371	353	392	0	-16	0	0.6869
NTw1AZ	46	414	394	448	0	-18	0	0.6693
NTw1AZ	60	459	441	503	0	-20	0	0.6514

For the anisotropic foam the three diagonal values will in general all be different, and the dynamic drag impedance tensor will have off-diagonal components. The magnitudes of both diagonal components and off diagonal components increase with increasing anisotropy. The degree of anisotropy is related to the twist angle.

3.4 Anisotropic elastic properties

For all the simulation results of the the equivalent Hooke's tensor discussed in the present work, the inverse estimation for an $30 \times 30 \times 30$ cellular array has been performed. The details of the inverse estimation process, e.g. convergence behaviour, number of iterations, residual errors, etc. will not be discussed in the present work and the reader is directed to [10, 11] for background information. In the present investigation, the focus is on the equivalent homogeneous linear elastic static properties of the cellular material. For this purpose, using the engineering order of the stress-strain components, the constitutive equation is in the form of the generalised Hooke's law given by

$$\boldsymbol{\sigma} = \mathbf{C}\boldsymbol{\varepsilon} \tag{16a}$$

$$\boldsymbol{\sigma} = \{\sigma_{11}, \sigma_{22}, \sigma_{33}, \sigma_{12}, \sigma_{13}, \sigma_{23}\}^T \tag{16b}$$

$$\boldsymbol{\varepsilon} = \{\varepsilon_{11}, \varepsilon_{22}, \varepsilon_{33}, 2\varepsilon_{12}, 2\varepsilon_{13}, 2\varepsilon_{23}\}^T \tag{16c}$$

where $\mathbf{C}$ is the Hooke's matrix associated with the stiffness form of Hooke's law, $\boldsymbol{\sigma}$ is the stress vector, $\boldsymbol{\varepsilon}$ is the strain vector and indices 1, 2 and 3 respectively denote the X, Y and Z axis of the global reference Cartesian coordinate system. In the general case of a fully anisotropic elastic material, 21 independent elastic constants are required in the Hooke's matrix. Following [10, 11, 22], the elastic moduli are normalised with respect to C_{33}^{REF}, such that $\hat{C}_{ij} = C_{ij}/C_{33}^{REF}$:

$$\mathbf{C} = C_{33}^{REF} \begin{bmatrix} \hat{C}_{11} & \hat{C}_{12} & \hat{C}_{13} & \hat{C}_{14} & \hat{C}_{15} & \hat{C}_{16} \\ & \hat{C}_{22} & \hat{C}_{23} & \hat{C}_{24} & \hat{C}_{25} & \hat{C}_{26} \\ & & \hat{C}_{33} & \hat{C}_{34} & \hat{C}_{35} & \hat{C}_{36} \\ & & & \hat{C}_{44} & \hat{C}_{45} & \hat{C}_{46} \\ & & sym & & \hat{C}_{55} & \hat{C}_{56} \\ & & & & & \hat{C}_{66} \end{bmatrix}. \tag{17}$$

where $C_{33}^{REF} = 13.8$ MPa is the C_{33} of the REF structure, and the respective equivalent Young's modulus $E^{REF} = 7.06$ MPa, as given in [10, 11].

4 Validation of panel with isotropic material

The modified code was validated by first comparing a characterized Biot material used state space transfer matrix method compared to the traditional transfer matrix method as implemented in the commercial software Maine3A from Université du Maine. Identical results were found when the same input from normal incidence is used. The data of the selected porous foam is given in Table 2. The panel on the incident side was 0.7 mm steel and on the other side 1.2 mm aluminium. The thickness of the foam was 30 mm. The stiffness of the isotropic foam was estimated in the same way for all cases: Young's modulus of 0.14 MPa, Poisson's ratio of 0.3 and foam structural loss factor of 0.1. Normal incidence is used for the validation case.

Table 2: Isotropic material for validation. Identical stiffness data was used in both cases. Note: for the micro material the dynamic drag impedance was estimated at 20 Hz.

Material	ρ_1	ρ_s	σ_0	ϕ	Λ	Λ'	$\alpha_{\inf}$	R_0	h_c
unit	kg/m^3	kg/m^3	Ns/m^4	–	μm	μm	–	μm	mm
Maine3A foam	25	N/A	15000	0.98	100	250	1.05	N/A	N/A
Micro material	24.9	1574	15516*	0.984	101	214	N/A	3.8	0.21

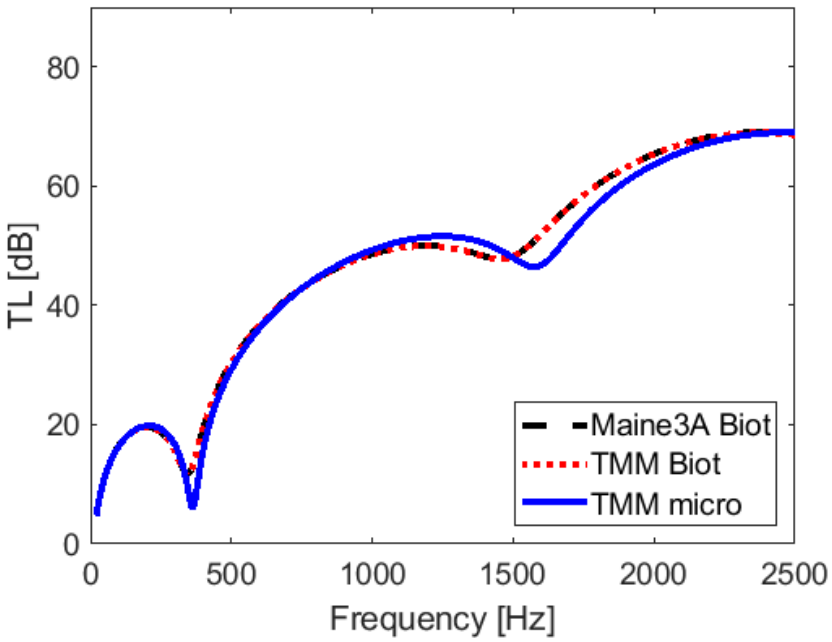

Figure 3: Transmission loss calculated with Maine3A, state-space TMM code with Biot formulation and state space TMM code with micro formulation

A micro geometry that would give the porosity and dynamic drag impedance close to the characterized foam was estimated. After that it was verified that the viscous and thermal characteristic lengths would be roughly of the right order of magnitude. Since the JCA parameters are interdependent not all parameters can be exact, in particular if a foam with nonzero pore size dispersion is approximated with a periodic micro structure [23]. The viscous characteristic length was approximated with twice the pore size and the thermal characteristic

length was estimated by the pore volume divided by the wetted surface of the unit cell. L denotes the strut length.

$$\Lambda = 2(h_c - 2R_0) \tag{18}$$

$$\Lambda' = 2\phi\frac{8\sqrt{2}L^3}{24\pi 2R_0 L} \tag{19}$$

The Biot calculation of transmission loss agrees completely between the state space TMM Biot formulation and Maine3A Biot implementation. The micro formulation agrees very well with them both up to about 1000 Hz. The discrepancy at higher frequencies is due to the equivalent mass of the foam being slightly less mass than the actual foam. The equivalent bulk modulus in the micro model gives the stiffness of the air in the in addition to the structural stiffness. The equivalent bulk modulus for the micro material is somewhat higher than in the Biot calculations. Possible explanations for the mass difference include that the assumed isotropic micro-structure is not a perfect match for the actual micro-structure, and that with the assumed properties the porosity is probably on the high side (0.984). The solid density is not given explicitly in the reference case in Maine3A, but it is set to 1574 kg/m^3, which is a typical value for Melamine foam. The micro model acoustic bulk modulus is assumed to be a constant material property modified only by the porosity and the thermal factor χ [20], not a frequency dependent quantity as in the JCA model of the Biot material. Therefore there is not a one to one correspondence between the two different bulk modulus values at higher frequencies.

5 Sound transmission loss for a panel including anisotropic foam

In order to calculate the sound transmission loss of the composite panel including ansiotropic foam a state space formulation of the transfer matrix method based on the $\{\boldsymbol{u}^s\boldsymbol{u}^t\}$ formulation is used. The code developed by Parra Martinez et al. following [2] and [24] has been extended to include the acoustic properties of micro modelled foams using the expressions presented in the previous section. In the extended code the micro geometry based equations 9 ,10 and 11 have been implemented directly using the dynamic drag impedance $\boldsymbol{Z}$ estimated from micro geometry parameters.

To investigate if anisotropic foams can bring added value to the sound transmission loss of typical enclosure design consisting of 1 mm perforated polymer panel, 30 mm foam and a 0.8 mm steel is analyzed. The model is shown in Figure 4.

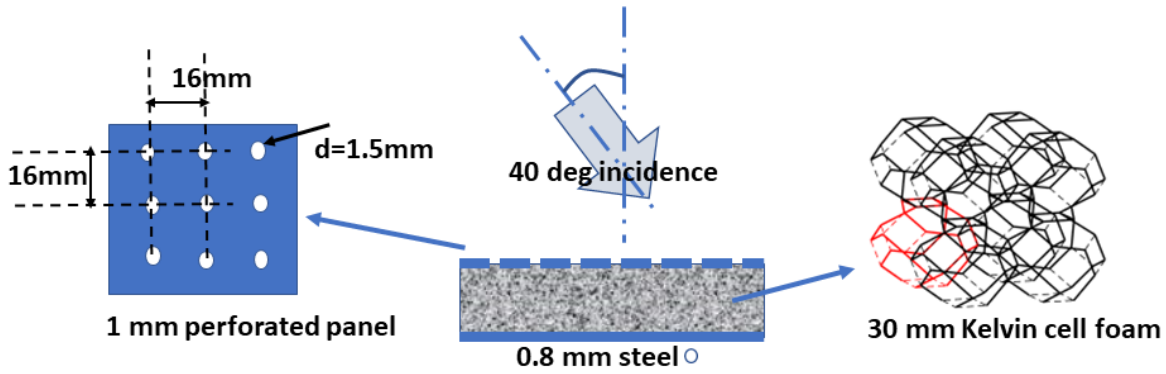

Figure 4: Example used for calculating transmission loss with anisotropic foam including a perforated polymer panel, 30 mm anisotropic foam and 0.8 mm steel.

The foam is modelled with several different degrees of anisotropy, but always with the same cell height and strut thickness. The porosity will vary due to that the twisted cells will be denser than the isotropic cell. The isotropic foam is modelled including the calculated stiffness from inverse estimation [11] . In addition,

the anisotropic case is compared to a case using the closest isotropic stiffness using minimum log-Euclidean distance according to Norris [25] as an approximation of the anisotropic stiffness.

Table 3: Material properties

	symbol	foam	perforated panel	unit
fluid density	ρ_f	1.2044	1.2044	kg/m^3
solid density	ρ_s	1600	1250	kg/m^3
fluid dynamic viscosity	μ_f	1.8140 $\times 10^{-5}$	1.8140 $\times 10^{-5}$	kg/ms
fluid bulk modulus	K_f	101325	101325	Pa
fluid thermal conductivity	κ_f	0.02577	0.02577	W/m K
solid thermal conductivity	κ_s	0.16	0.16	W/m K
fluid specific heat	C_{pf}	1005	1005	J/kg K
solid specific heat	C_{ps}	1600	1600	J/kg K
fluid expansion coefficient	η	3.43 $\times$ 10^{-3}		-
solid Young's modulus	E_s	563$\times$ 10^6	563$\times$ 10^6	Pa
solid Poisson's ratio	ν	0.3	0.3	–
open cell porosity	ϕ	0.65-0.70	0.00276	–

The densities, porosities and Hooke's tensor component C33 across the panel thickness is given in tables 4 and 5. For the case of 60° of twist, the TL is compared to the isotropic case, and an isotropic case with the isotropic stiffness replaced by the closest isotropic stiffness. As can be seen in Figure 6, the closest isotropic model fails to capture the essential behaviour of the anisotropic design, even if the density of the foam is adjusted to the same as that of the twisted foam. In Table 3 the material properties for the foam and the perforated panel are given. The steel is modelled as an isotropic solid with density 7800 kg/m^3 Young's modulus 2×10^{11} Pa, Poisson's ratio of 0.3 and a structural loss factor $\eta = 0.01$.

Table 4: Test cases for transmission loss including foam stiffness. The dynamic drag impedance for the corresponding cases is given in Table 1.

Case	micro model	twist [°]	porosity –	C_{33} [MPa]	foam density [kg/m^3]
ISO	KC ISO	0	0.70	13.8	476
TL30	NTw1Az	30	0.69	8.38	501
TL46	NTw1Az	46	0.67	5.73	529
TL60	NTw1Az	60	0.65	4.11	558
ISO approx. of TL60	closest iso	0	0.70	6.45	476
Heavy ISO approx. of TL60	closest iso	0	0.70	6.45	558

Table 5: Hooke's tensor components for isotropic, anisotropic cases and the closest isotropic tensor to the case with 60° twist. $\hat{C}_{ij} = C_{ij}/C_{33}^{REF}$ where C_{33}^{REF} is 13.8 MPa.

model	twist	$\hat{C}_{33} = C_{33}/C_{33}^{REF}$	$[\hat{C}_{11}, \hat{C}_{22}]$	$[\hat{C}_{12}, \hat{C}_{13}, \hat{C}_{23}]$	$[\hat{C}_{44}, \hat{C}_{55}, \hat{C}_{66}]$
ISO	0°	1.0	[1, 1, 1]	[0.63, 0.63, 0.63]	[0.18, 0.18, 0.18]
NTw1Az	30°	0.61	[0.71, 0.71]	[0.28, 0.32, 0.32]	[0.18, 0.16, 0.16]
NTw1Az	46°	0.42	[0.63, 0.63]	[0.13, 0.20, 0.20]	[0.17, 0.15, 0.15]
NTw1Az	60°	0.30	[0.60, 0.60]	[0.45, 0.13, 0.13]	[0.17, 0.14, 0.14]
Closest ISO to 60°	0°	0.44	[0.44, 0.44]	[0.13, 0.13, 0.13]	[0.16, 0.16, 0.16]

6 Results

The resulting transmission loss for the anisotropic foams with twist angles 0° (isotropic), 30°, 46° and 60° is shown in Figure 5. The effect of the reduced stiffness from Table 5 of lowering the frequency of maximum transmission loss is clearly seen.

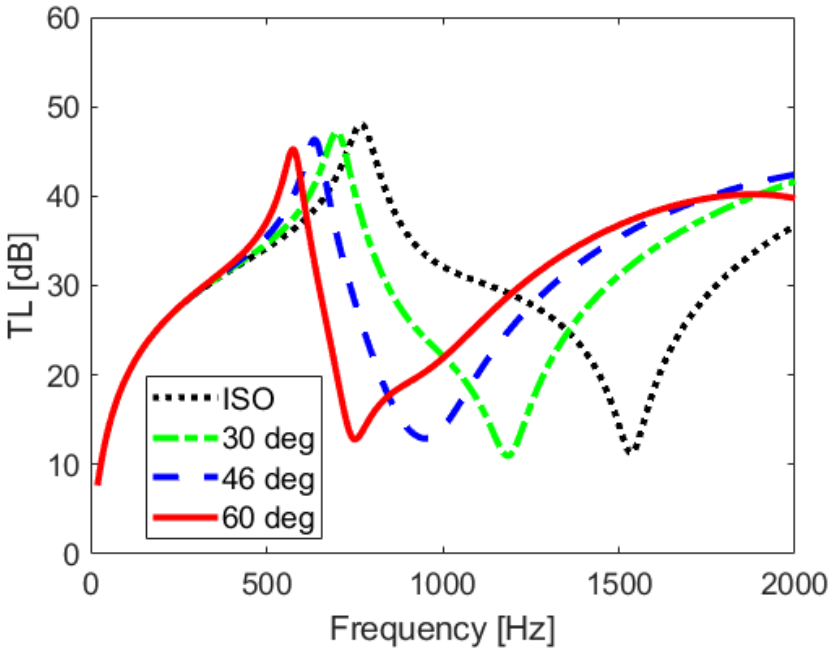

Figure 5: Calculated transmission loss for increasing degree of twist.

The curves shown in Figure 6 demonstrates that the anisotropic micro foams are less stiff than the isotropic micro foam as can be seen in Mao et. al. [11]. The fundamental resonance occurs at increasingly lower frequencies the more twisted the micro geometry is. In Table 4 the value of the Hooke's tensor in the thickness direction is given for comparison and the stiffness is decreasing from 13.8 MPa for the isotropic Kelvin cell model down to 30% of the isotropic value, or 4.59 MPa for the NTw1AZ cell which has 60° of twist angle. At the same time the in plane stiffness C_{11} and C_{22} are 60% of the isotropic reference value. The in plane stiffness is thus twice as high as the out of plane stiffness. This high degree of anisotropy cannot be captured by an isotropic model.

The shift of the peak in transmission loss to lower frequencies could in addition to the lowered stiffness also be caused by the increase of foam weight as the more anisotropic foams have lower porosity. To investigate this influence the cases of closest isotropic stiffness is compared to the anisotropic case with 60° twist. The foam input data is given in Table 4. The case named 'heavy closest iso' refers to a foam with stiffness corresponding to the closest isotropic stiffness to the NTw1AZ case with 60° twist and having the same surface mass as the anisotropic foam with a 60° twist. In Figure 6 it can be observed that although the heavy closest isotropic case does give a small shift to lower frequencies, it still cannot full model the behaviour of the anisotropic design.

7 Discussion

A study of transmission loss of a sandwich type design with a layer of anisotropic foam based on a Kelvin cell micro-geometry has been presented. It it shown how the stiffness of the foam will vary related to the amount of twist applied to the fundamental isotropic Kelvin Cell micro geometry. Since the stiffness is directly related to the degree of anisotropy and the amount of twist applied, the frequency characteristics of the

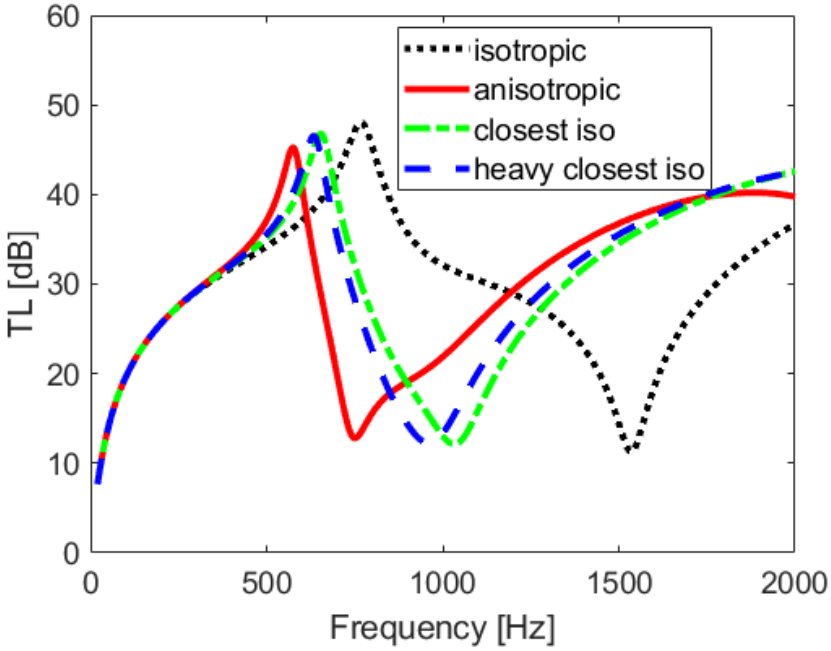

Figure 6: Comparison of calculated TL for isotropic, fully anisotropic with 60° twisted micro cells and closest isotropic stiffness. The heavy closest isotropic foam has the same mass as the fully anisotropic foam with 60° twist and the closest isotropic stiffness.

narrow-band transmission loss can be tuned. In particular it is possible to shift the frequency of maximum transmission loss to lower frequencies by including this type of anisotropic foam. This can provide an opportunity to have higher transmission loss at the frequencies where it has best effect, i.e. at frequencies where the source excitations are expected to be high.

To fully capture the frequency dependence it seems necessary to model the foam as anisotropic, as is shown in Figure 6. Even when the closest isotropic stiffness is used to approximate the anisotropic foam, and the weight is increased to match the anisotropic design, the prediction of the narrowband transmission loss loses accuracy.

Since the more twisted porous designs have a lower porosity than the isotropic porous material the anisotropic layer will increase in surface weight. The corresponding surface weight increase of the total multi-layer design is 3.4%, 7.3% and 11.8% for cases with 30°, 46° and 60° of twist respectively. The indication is that by exploiting the characteristics of anisotropic porous materials transmission loss improvements in particular at lower frequencies are possible for sandwich type designs. The improvements are obtained with the same build height and a very moderate weight increase. An important benefit with the anisotropic porous material is the possibility to tune the fundamental resonances and frequency of maximum transmission loss without having to change the build height or thicknesses of load carrying structures, which often are subject to design constraints.

8 Conclusion

By using an anisotropic open porous material in a multi-layer panel, there is a possibility of tuning sound transmission loss at lower frequencies without adding thickness and by adding limited surface weight. The frequency of maximum transmission loss is shifted to lower frequencies due to the lower stiffness of the anisotropic porous material compared to the isotropic porous material. However, these vibro-acoustic properties cannot be fully captured unless the material is modelled as anisotropic. Even if the closest isotropic stiffness is used instead of the anisotropic stiffness and the mass of the micro-modelled Kelvin cell foam

layer is the same as in the anisotropic model, the approximate isotropic model cannot fully estimate the transmission loss behaviour as a function of frequency. The stiffness properties of the model need to be estimated using inverse estimation of finite element calculations, but the acoustic properties can be assessed with much less computational effort using an analytical approach based on the basic micro geometry of the open cell foam.

Acknowledgements

The authors are gratefully acknowledging the support from the Centre of ECO2 Vehicle Design funded by Swedish Innovation Agency Vinnova (Grant number 2016-05195). Eva Lundberg would also like to thank Volvo Construction Equipment for supporting this contribution. The Swedish Research Council (VR Grants No. 2021-05791) is also gratefully acknowledged for its financial support.

References

[1] O. Dazel, J.-P. Groby, B. Brouard, and C. Potel, "A stable method to model the acoustic response of multilayered structures," *Journal of Applied Physics*, vol. 113, p. 083506, 2013.

[2] J. P. Parra Martinez, O. Dazel, P. Göransson, and J. Cuenca, "Acoustic analysis of anisotropic poroelastic multilayered systems," *Journal of Applied Physics*, vol. 119, no. 8, p. 84907, 2016.

[3] W. Thomson, "Transmission of elastic waves through a stratified solid medium," *Journal of Applied Physics*, vol. 21, no. 2, pp. 89–93, 1950.

[4] N. Haskell, "The dispersion of surface waves in multi-layered media," *Bulletin of the Seismological Society of America*, vol. 43, no. 17, 1953.

[5] C. V. der Kelen and P. Göransson, "Identification of the full anisotropic flow resistivity tensor for multiple glass wool and melamine foam samples," *The Journal of the Acoustical Society of America*, vol. 134, pp. 4659 –4669, 2013.

[6] A. Huber and L. Gibson, "Anisotropy of foams," *Journal of materials science*, vol. 23, no. 8, pp. 3031–3040, 1988.

[7] N. Jonkers, W. Dijk, N. Vonk, J. Van Dommelen, and M. Geers, "Anisotropic mechanical properties of selective laser sintered starch-based food," *Journal of Food Engineering*, vol. 318, p. 110890, 11 2021.

[8] T. Cavalieri, J. Boulvert, G. Gabard, V. Romero-García, M. Escouflaire, J. Regnard, and J.-P. Groby, "Graded and anisotropic porous materials for broadband and angular maximal acoustic absorption," *Materials*, vol. 13, p. 4605, 10 2020.

[9] H. T. Luu, C. Perrot, and R. Panneton, "Influence of porosity, fiber radius, and fiber orientation on anisotropic transport properties of random fiber structures," *The Journal of the Acoustical Society of America*, vol. 141, no. 5, pp. 3888–3888, 2017.

[10] H. Mao, R. Rumpler, and P. Göransson, "An inverse method for characterisation of the static elastic hooke's tensors of solid frame of anisotropic open-cell materials," *International Journal of Engineering Science*, vol. 147, p. 103198, 2020.

[11] H. Mao, R. Rumpler, M. Gaborit, P. Göransson, J. Kennedy, D. O'Connor, D. Trimble, and H. Rice, "Twist, tilt and stretch: From isometric kelvin cells to anisotropic cellular materials," *Materials & Design*, vol. 193, p. 108855, 2020.

[12] V. H. Trinh, V. Langlois, J. Guilleminot, C. Perrot, Y. Khidas, and O. Pitois, "Tuning membrane content of sound absorbing cellular foams: Fabrication, experimental evidence and multiscale numerical simulations," *Materials & Design*, vol. 162, pp. 245 – 361, 2020.

[13] O. Dazel, B. Brouard, C. Depollier, and S. Griffiths, "An alternative boit's displacement formulation for porous materials." *The Journal of the Acoustical Society of America*, vol. 121, no. 6, pp. 3509 – 3516, 2007.

[14] B. Semeniuk and P. Göransson, "Microstructure based estimation of the dynamic drag impedance of lightweight fibrous materials," *The Journal of the Acoustical Society of America*, vol. 141, no. 3, pp. 1360–1370, 2017.

[15] B. Semeniuk, P. Göransson, and O. Dazel, "Microstructure based modelling of the thermal and viscous dissipation of a transversely isotropic porous fibrous insulation material," in *Proc. of ISMA 2018 and USD 2018, International Conference on Noise and Vibration Engeineering , Leuven, Belgium, (September 17-19, 2018)*, 2018.

[16] W. E. Warren and A. M. Kraynik, "Linear elastic behavior of a low-density kelvin foam with open cells," *Journal of applied mechanics*, vol. 64, no. 4, pp. 787–794, 1997.

[17] H. Zhu, J. Knott, and N. Mills, "Analysis of the elastic properties of open-cell foams with tetrakaidecahedral cells," *Journal of the Mechanics and Physics of Solids*, vol. 45, no. 3, pp. 319–343, 1997.

[18] R. M. Sullivan and L. J. Ghosn, "Shear moduli for non-isotropic, open cell foams using a general elongated kelvin foam model," *International journal of engineering science*, vol. 47, no. 10, pp. 990–1001, 2009.

[19] E. Lundberg, B. Semeniuk, and P. Göransson, "Simplified acoustic model of an anisotropic foam using a micro-macro approach," in *Proc. of ISMA 2020 and USD 2020, International Conference on Noise and Vibration Engeineering , online, (September 7-9, 2020)*, 2020.

[20] B. P. Semeniuk, P. Göransson, and O. Dazel, "Dynamic equations of a transversely isotropic, highly porous, fibrous material including oscillatory heat transfer effects," *The Journal of the Acoustical Society of America*, vol. 146, no. 4, pp. 2540–2551, 2019.

[21] M. He, C. Perrot, J. Guilleminot, P. Leroy, and G. Jacqus, "Multiscale prediction of acoustic properties for glass wools: Computational study and experimental validation," *The Journal of the Acoustical Society of America*, vol. 143, no. 6, pp. 3283–3299, 2018.

[22] H. Mao, M. Gaborit, E. Lundberg, R. Rumpler, B. Yin, and P. Göransson, "Dynamic behaviour of low- to high-density anisotropic cellular materials," *Journal of Sound and Vibration*, 2022, doi=https://doi-org.focus.lib.kth.se/10.1016/j.jsv.2022.117137.

[23] K. V. Horoshenkov, J.-P. Groby, and O. Dazel, "Asymptotic limits of some models for sound propagation in porous media and the assignment of the pore characteristic lengths," *The Journal of the Acoustical Society of America*, vol. 139, no. 5, pp. 2463–2474, 2016.

[24] P. G. J.P. Parra Martinez, O. Dazel and J. Cuenca, "Derivation of the state matrix for dynamic analysis of linear homogeneous media," *The Journal of the Acoustical Society of America*, vol. 140, no. 2, pp. EL218n – EL220, 2016.

[25] A. N. Norris, "The isotropic material closest to a given anisotropic material," *Journal of mechanics of materials and structures*, vol. 1, no. 2, pp. 223–238, 2006.